Statistical Properties and Airspace Capacity for Unmanned Aerial Vehicle Networks Subject to Sense-and-Avoid Safety Protocols

Mushuang Liu, Yan Wan, *Senior Member, IEEE*, Frank L. Lewis, *Life Fellow, IEEE*, Ella Atkins, *Senior Member, IEEE*, and Dapeng Oliver Wu, *Fellow, IEEE*

***Abstract*— Random mobility models (RMMs) capture the random mobility patterns of mobile agents, and have been widely used as the modeling framework for the evaluation and design of mobile networks. All existing RMMs in the literature assume independent movements of mobile agents, which does not hold for unmanned aircraft systems (UASs). In particular, UASs must maintain a safe separation distance to avoid collision. In this paper, we propose a new modeling framework of random mobility models equipped with physical sense-and-avoid protocols to capture the flexible, variable, and uncertain movement patterns of UASs subject to separation safety constraints. For the random direction (RD) RMM equipped with a commonly used sense-and-avoid (S&A) protocol, named sense-and-stop (S&S), we provide its statistical properties including stationary location distribution and stationary inter-vehicle distance distribution, using the Markov analysis. This study provides knowledge on the impact of S&A protocols to critical UAS networking statistics. In addition, we define collision probabilities and airspace capacity concepts for UASs based on the inter-vehicle distance distribution, and derive their closed-form expressions. This analytical framework mathematically bridges local autonomy with global airspace capacity, and allows the impact analysis of local autonomy configurations for effective UAS airspace capacity management.**

***Index Terms*— Random mobility model, sense and avoid, collision avoidance, aerial networking, unmanned aircraft system traffic management, airspace capacity management.**

I. Introduction

UNMANNED aircraft system (UAS) technology has demonstrated its value in broad commercial applications, such as sports coverage, cargo transport, precision agriculture, public safety, on-demand communication provision, and structure health monitoring [2]–[7]. The global commercial UAS Market is projected to reach $52.30 billion by 2025 [8]. With the new, small UAS rules released by the Federal Aviation Administration (FAA) in August 2016 [9], we foresee a dense UAS use in the National Airspace System (NAS). Along with this trend, new research directions that deal with multiple UASs in a dense airspace become urgent, such as UAS traffic management (UTM) and UAS networking.

UTM is very different from traditional air traffic management (ATM) [10], [11]. Unlike commercial flights which have pre-defined flight plans and rather deterministic flight trajectories, UASs in the low-altitude airspace are featured by their highly flexible, variable and uncertain movement patterns. Such features unique to UASs constitute the leading challenge for UAS traffic analysis. Concepts such as "highway in the sky" are borrowed from traditional ATM to simplify the UTM architecture, however, such "infrastructure" limits UAS flexibility and contradicts their on-demand missions. Little is known about the limitations of airspace capacity subject to highly flexible UAS operations. Related to our interest, a capacity concept for UTM was proposed in [12], which assumes unified flow directions for all UASs. In [13], a phase-transition-based capacity concept was proposed based on simulation studies of randomly generated source-to-destination UAS trajectories.

To understand the capacity limit of UAS traffic subject to highly flexible, variable and uncertain UAS movement patterns, we develop a new random mobility model (RMM) -based modeling and analytical framework. RMMs have been widely used for networking studies. Examples include Random Direction (RD), Random Walk (RW), Guass-Markov (GM), and Smooth Turn (ST) developed specifically for fixed-wing UASs [14]–[19]. Please refer to our survey paper [14] on the RMMs developed for different UAS applications ranging from search, rescue, and reconnaissance, to patrolling, cargo, and AN backbone. These RMMs capture the random mobility patterns of moving agents, and have commonly been used as the evaluation and design foundation of mobile ad hoc networks (MANET), vehicular ad hoc networks (VANET), and UAS networks (or called flying ad hoc networks, FANET), from which important statistics can be derived, such as node distribution, inter-vehicle distance distribution, and link/path lifetime [20], [21].

We note that all these existing RMM studies assume that mobile agents move independently. This assumption does not hold for UASs. In particular, in order to maintain airspace safety, UASs must be equipped with sense and avoid (S&A) capabilities. This S&A feature is a critical

Manuscript received March 16, 2020; revised July 28, 2020; accepted September 8, 2020. Date of publication December 11, 2020; date of current version September 1, 2021. This work was supported by the National Science Foundation under Grant 1714519 and Grant 1730675. The Associate Editor for this article was D. Sun. *(Corresponding author: Yan Wan.)*

Mushuang Liu and Yan Wan are with the Department of Electrical Engineering, The University of Texas at Arlington, Arlington, TX 76019 USA (e-mail: yan.wan@uta.edu).

Frank L. Lewis is with the UTA Research Institute, University of Texas at Arlington, Fort Worth, TX 76118 USA.

Ella Atkins is with the Department of Aerospace Engineering, University of Michigan, Ann Arbor, MI 48109 USA.

Dapeng Oliver Wu is with the Department of Electrical and Computer Engineering, University of Florida, Gainesville, FL 32611 USA.

Digital Object Identifier 10.1109/TITS.2020.3040520

difference between FANET and MANET. S&A fundamentally changes the statistics for networking, and its impact is not known. In this paper, we develop an analytical framework of RD RMMs equipped with S&A protocols, analyze its statistical performance, and then connect it to airspace capacity concept to understand the limit of airspace capacity. We note that the analysis here is much more complicated when the independent movement assumption does not hold any more.

The contributions of this paper are listed as follows.

1) We develop a new modeling and analytical framework for UTM and UAS networking studies. In the framework, RMMs are equipped with physical S&A protocols to succinctly capture the flexible, variable, and uncertain movement patterns of UASs subject to separation safety constraints. This framework, first of its kind per knowledge of the authors, merges advances in UAS communication and networking studies with UAS physical safety constructs for UTM studies.
2) For the new RD RMM equipped with a S&A protocol, named sense-and-stop (S&S), we develop statistics that are critical to networking studies, namely stationary node distribution and stationary inter-vehicle distance distribution, using the Markov analysis.
3) We define stationary collision probabilities for UASs based on the inter-vehicle distance distribution, and derive their expressions. This new stationary collision probability construct quantifies the effectiveness of S&A protocols.
4) We define UAS airspace capacity based on stationary collision probabilities, and derive their expressions. This new UAS airspace capacity concept captures the flexibility of UAS operations as it only relies on the S&A protocols to maintain airspace safety, with no other physical mobility constraints being enforced. This capacity concept provides us insight on the limitation of airspace density for highly flexible and autonomous UASs, which is very different from that for traditional air traffics.
5) The impact of local S&A protocols on global airspace capacity is studied. This analysis bridges local autonomy with global airspace capacity, and permits insightful impact analysis of local autonomy configurations, e.g., randomness level of a RMM, sensing distance, and collision distance, to achieve effective UAS airspace capacity management.

The remainder of this paper is organized as follows. Section II describes both the independent RD RMM and the RD RMM equipped with the S&S protocol. Section III analyzes the statistical properties of both RMMs in terms of node distribution and inter-vehicle distance distribution. Section IV analyzes the collision probabilities and airspace capacity for both RMMs. Section V includes the impact analysis of model configurations. Simulation studies are included throughout the paper to help illustrate the analytical results. Section VI concludes the paper.

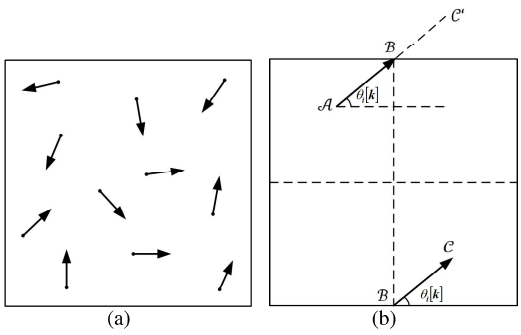

Fig. 1. Illustration of (a) a 2-D airspace with UAS mobility captured by the independent RD RMMs, and (b) the wrap-around boundary model.

II. The Modeling Framework

This section describes the modeling framework of UAS operations. To capture the highly flexible, variable, and uncertain movement patterns of UASs, we use the RD RMM -based modeling framework, which is described in Section II-A. To capture the safety constraints of flexible UAS operations, we then equip the RD RMM with the S&S protocol in Section II-B.

A. Independent Random Direction Mobility Model

In the independent RD RMM widely used in the literature, UASs travel independently in an airspace $[0, B)^2$ (Figure 1(a)). A comprehensive description of RMMs used for UASs can be found in the survey paper [14]. At each time instant $1, 2, \ldots, k$, UAS i selects a heading direction $\Theta_i[k]$ from $[0, 2\pi)$ randomly, and moves along that direction with a constant heading speed V. $\Theta_i[k]$ is uniformly distributed in $[0, 2\pi)$, $\forall i, k$, i.e., the probabilistic density function (pdf) of $\Theta_i[k]$ is

$$f(\Theta_i[k] = \theta) = \frac{1}{2\pi}. \tag{1}$$

$X_i[k]$ and $Y_i[k]$ denote the stochastic processes for UAS i's location along the x and y axes.

We use the widely adopted wrap-around boundary model to avoid the border effect [15]. When a UAS hits the boundary, it wraps around and appears at the opposite side with the same velocity and heading direction (Figure 1(b)). This wrap-around model is suitable for large simulation regions and is analysis-friendly. With this boundary model, the dynamics of UAS i can be described as

$$X_i[k] = X_i[k-1] + V\cos\Theta_i[k-1] - B\left\lfloor \frac{X_i[k-1] + V\cos\Theta_i[k-1]}{B} \right\rfloor, \tag{2}$$

$$Y_i[k] = Y_i[k-1] + V\sin\Theta_i[k-1] - B\left\lfloor \frac{Y_i[k-1] + V\sin\Theta_i[k-1]}{B} \right\rfloor, \tag{3}$$

where $\lfloor . \rfloor$ is the floor function.

In the wrap-around boundary model, the cyclic relative position of the UAS pair i and j along x axis (y axis) takes the smaller value of $|X_i[k] - X_j[k]|$ and $B - |X_i[k] - X_j[k]|$

$\big(|Y_i[k] - Y_j[k]|$ and $B - |Y_i[k] - Y_j[k]|\big)$. Interested readers please refer to the detailed descriptions of cyclic relative position in the wrap-around boundary model in [22]–[24]. Mathematically, the inter-vehicle cyclic relative position $S_{i,j}[k] = (\Delta X_{i,j}[k], \Delta Y_{i,j}[k])$ and distance $D_{i,j}[k]$ between two UASs i and j at time k are calculated as:

$$\begin{aligned}\Delta X_{i,j}[k] &= \min(|X_i[k] - X_j[k]|, B - |X_i[k] - X_j[k]|),\\ \Delta Y_{i,j}[k] &= \min(|Y_i[k] - Y_j[k]|, B - |Y_i[k] - Y_j[k]|),\\ D_{i,j}[k] &= (\Delta X_{i,j}[k]^2 + \Delta Y_{i,j}[k]^2)^{\frac{1}{2}}.\end{aligned} \tag{4}$$

B. Random Direction Mobility Model Equipped With the S&S Protocol

Safety constraints are critical for UAS operations. The FAA "right-of-way" rules state that for vehicles of the same category and operating at the same altitude, the aircraft to the right has the right-of-way [9]. In the literature, many papers focus on the development of S&A safety protocols when two UASs encounter (see e.g., [25]–[28]). However, the successful collision avoidance between two UASs may lead to a collision that involves other UASs in a dense airspace. As such, it is the purpose of this paper to exploit the relationship between local S&A protocol's impact and global airspace capacity.

Here, we implement a "right-of-way" rule, named 'sense-and-stop" (S&S), similar to the hovering strategy [29]. Denote the sensing distance (or observing distance) as d_o, which is much smaller than $\frac{B}{2}$. The RD RMM equipped with S&S protocol works as follows: a) when the inter-vehicle distance between two UASs is greater than sensing distance, i.e., $D_{i,j}[k] > d_o$, each UAS moves independently according to the independent RD RMM; b) when $D_{i,j}[k] \leq d_o$, the vehicle to the left (i.e., with a smaller x location) stops, and the other vehicle follows the independent RD RMM until $D_{i,j}[k] > d_o$. When multiple UASs are involved, they are considered as a collection of UAS pairs. For any UAS i, if the following stopping criterion $\mathcal{C}_i$ is true then UAS i stops: there exists a UAS j ($j \neq i$) such that $D_{i,j}[k] \leq d_o$ and $X_i[k] < X_j[k]$. If the stopping criterion $\mathcal{C}_i$ is not met, then the UAS i moves with independent RD RMM. The dynamics of UAS i can thus be described as follows.

$$X_i[k] = \begin{cases} X_i[k-1], & \mathcal{C}_i \text{ is true},\\ X_i[k-1] + V\cos\Theta_i[k-1] & \\ \quad -B\left\lfloor \dfrac{X_i[k-1] + V\cos\Theta_i[k-1]}{B} \right\rfloor, & \mathcal{C}_i \text{ is not true}, \end{cases} \tag{5}$$

$$Y_i[k] = \begin{cases} Y_i[k-1], & \mathcal{C}_i \text{ is true},\\ Y_i[k-1] + V\sin\Theta_i[k-1] & \\ \quad -B\left\lfloor \dfrac{Y_i[k-1] + V\sin\Theta_i[k-1]}{B} \right\rfloor, & \mathcal{C}_i \text{ is not true}. \end{cases} \tag{6}$$

In addition, for any UAS i, if there exists a UAS j satisfying $D_{i,j}[k] \leq d_o$ and $X_i[k] = X_j[k]$, then a small noise is added to $X_i[k]$ to differentiate their locations in x coordinate. As there always exists a UAS with the maximal x location, we can ensure that at least one UAS moves at each time instant k in the airspace and the dead-lock phenomenon does not occur.

III. Analysis of Network Statistics

In this section, we study the statistical properties of both RD RMMs critical to networking and UTM studies, in terms of stationary node distribution and inter-vehicle distance distribution.

A. Stationary Node Distribution

Define node distribution as the joint distribution of UAS locations and heading directions. Lemma 1 studies the stationary node distribution for the independent RD RMM.

Lemma 1: Each of the N UASs in an airspace $[0, B)^2$ moves independently according to the RD RMM. The stationary node distribution of each UAS is uniform, i.e.,

$$\lim_{k\to\infty} f(X_i[k] = x, Y_i[k] = y, \Theta_i[k] = \theta) = \frac{1}{2\pi B^2}, \tag{7}$$

where $x \in [0, B)$, $y \in [0, B)$, $\theta \in [0, 2\pi)$, and $i = 1, 2, \cdots, N$.

The stationary joint node distribution of N UASs is also uniform, regardless of the initial joint node distribution.

Proof: Define a Markov process with states $\hat{S}_i^b[k] = (X_i[k], Y_i[k], \Theta_i[k])$ to represent the location and heading direction of UAS i moving with the independent RD RMM. The transition probability kernel of $\hat{S}_i^b[k]$ is $f^b(\hat{S}_i^b[k+1]|\hat{S}_i^b[k]) = \mathbf{1}\Big\{X_i[k] + V\cos\Theta_i[k] - B\Big\lfloor \frac{X_i[k]+V\cos\Theta_i[k]}{B}\Big\rfloor\Big\}\mathbf{1}\Big\{Y_i[k] + V\sin\Theta_i[k] - B\Big\lfloor \frac{Y_i[k]+V\sin\Theta_i[k]}{B}\Big\rfloor\Big\}\frac{1}{2\pi}$, where $\mathbf{1}\{.\}$ is 1 if $\{.\}$ is true and 0 if $\{.\}$ is false [15]. This Markov chain is aperiodic, Φ-irreducible, and Harris recurrent (refer to [30, Chapter 4] for formal definitions of these properties). Intuitively, this is because a) all states in the Markov chain are aperiodic according to Equations (2) and (3); b) all states communicate with each other; and c) all states are visited infinitely often when $k \to \infty$. Interested readers are referred to [15] for the formal mathematical proof of these properties. As such, there exists a unique stationary state distribution. As shown in [15, Proposition 4.2], the stationary node distribution for each UAS of independent RD RMM is uniform.

Because the N UASs move independently, the joint node distribution is a multiplication of N individual node distributions. A simple argument leads to the conclusion that the N UASs' stationary node distribution is uniform. □

The next theorem studies the stationary UAS location distribution for the RD RMM equipped with S&S protocol.

Theorem 1: Each of the N UASs in an airspace $[0, B)^2$ follows the RD RMM equipped with the S&S protocol. The stationary node distribution for each UAS i is uniform, regardless of the initial node distribution.

Proof: Define a Markov process with states $\hat{S}_i^S[k] = (X_i[k], Y_i[k], \Theta_i[k])$ to represent the location and heading direction of UAS i moving with the RD RMM equipped with the S&S protocol. Following a similar analysis as shown in Lemma 1, this Markov chain is aperiodic, Φ-irreducible, and Harris recurrent when N is finite, and therefore, there exists a unique stationary distribution [15]. To find the stationary location distribution of UAS i, we introduce a set $\mathcal{S}_s[k]$ to

hold all the locations of UAS i that satisfy the following condition: there exists a UAS j ($j \neq i$) satisfying $D_{i,j}[k] \leq d_o$ and $X_i[k] < X_j[k]$. $\bar{\mathcal{S}}_s[k]$ is the complement of $\mathcal{S}_s[k]$. The stationary location distribution along the x axis can be described as follows.

$$\begin{aligned}&\lim_{k\to\infty} f(X_i[k]=x)\\ &=\lim_{k\to\infty} f(X_i[k]=x|\bar{\mathcal{S}}_s[k])P(\bar{\mathcal{S}}_s[k])\\ &\quad+\lim_{k\to\infty} f(X_i[k]=x|\mathcal{S}_s[k])P(\mathcal{S}_s[k]).\end{aligned} \tag{8}$$

To prove $\lim_{k\to\infty} X_i[k]$ is uniformly distributed, we only need to show that $\lim_{k\to\infty} f(X_i[k] = x|\bar{\mathcal{S}}_s[k]) = \frac{1}{B}$ and $\lim_{k\to\infty} f(X_i[k]=x|\mathcal{S}_s[k]) = \frac{1}{B}$. The proof of the first statement $\lim_{k\to\infty} f(X_i[k] = x|\bar{\mathcal{S}}_s[k]) = \frac{1}{B}$ is straightforward using Lemma 1, as UAS i moves independently in this case. To prove the second statement, we note that as UAS i stops at time k, $\lim_{k\to\infty} f(X_i[k] = x|\mathcal{S}_s[k])$ is the same as the conditional probability right before the UAS enters the stop state. As UAS i moves randomly at that time step, the proof of the first statement leads to the conclusion that $\lim_{k\to\infty} f(X_i[k] = x|\mathcal{S}_s[k]) = \frac{1}{B}$. The proofs for the location along the y axis follow a similar argument. □

Remark 1: Although the location of each individual UAS is uniformly distributed for the RD RMM equipped with the S&S protocol, the joint distribution of N UAS locations is not uniform anymore. The introduction of the S&S protocol removes the independence of UAS trajectories, and alters the joint distribution. This new property is studied in Section III-B.

B. Stationary Inter-Vehicle Distance Distribution

In this section, we study the impact of the S&S protocol to stationary inter-vehicle distance distribution. Theorem 2 shows that the inter-vehicle relative position ($\Delta X_{i,j}$ and $\Delta Y_{i,j}$) distributions are uniform for the independent RD RMM, while this uniformity property does not hold for the RD RMM equipped with the S&S protocol as shown in Theorem 3.

Theorem 2: Each of the N UASs in an airspace $[0, B)^2$ moves independently according to the independent RD RMM. Then the following two statements hold.

a) The stationary distributions of the inter-vehicle relative positions, i.e., $\Delta X_{i,j}$ and $\Delta Y_{i,j}$, are uniform;

b)The stationary pdf of the cyclic inter-vehicle distance for two UASs i and j, $D_{i,j}[k]$, denoted as $f_D^b(d)$, is

$$\begin{aligned}f_D^b(d) &= \lim_{k\to\infty} f(D_{i,j}[k]=d)\\ &=\begin{cases}\dfrac{2\pi d}{B^2} & 0\leqslant d<\frac{B}{2}\\ \dfrac{4(\frac{\pi}{2}-2arccos(\frac{B}{2d}))d}{B^2} & \frac{B}{2}\leqslant d<\frac{\sqrt{2}B}{2}\end{cases}.\end{aligned} \tag{9}$$

Proof: Define a Markov process based on the cyclic relative position between the UAS i and j when they move with the independent RD RMM, $S^b[k] = (\Delta X_{i,j}[k], \Delta Y_{i,j}[k])$. As the deadlock phenomenon does not occur, the Markov chain $S^b[k]$ is aperiodic, Φ-irreducible, and Harris recurrent, and therefore, there exists a unique stationary distribution. We first calculate the pdfs for the stationary cyclic relative positions along the x and y axes, $\lim_{k\to\infty} f(\Delta X_{i,j}[k] = \Delta x)$ and $\lim_{k\to\infty} f(\Delta Y_{i,j}[k] = \Delta y)$. We remove the subscript i, j for the simplicity of presentation when it does not cause confusion. Equation (4) leads to

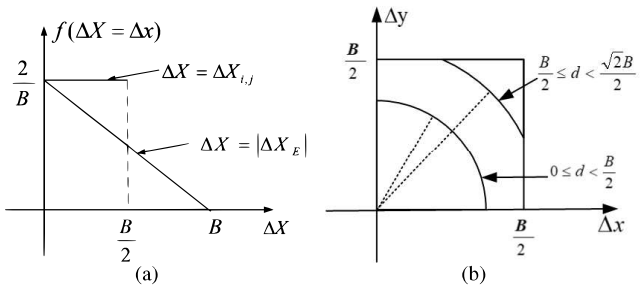

Fig. 2. (a). The relationship between pdfs for $|\Delta X_E[k]|$ and $\Delta X[k]$. (b). The range of cyclic distance D.

$$\begin{aligned}\Delta X[k] &= \begin{cases}|X_i[k]-X_j[k]| & |X_i[k]-X_j[k]|\leqslant\frac{B}{2}\\ B-|X_i[k]-X_j[k]| & |X_i[k]-X_j[k]|>\frac{B}{2}\end{cases}\\ &=\begin{cases}|\Delta X_E[k]| & |\Delta X_E[k]|\leqslant\frac{B}{2}\\ B-|\Delta X_E[k]| & |\Delta X_E[k]|>\frac{B}{2}\end{cases},\end{aligned} \tag{10}$$

where $\Delta X_E[k]$ is the Euclidean relative position between UASs i and j along the x axis, i.e., $\Delta X_E[k] = X_i[k] - X_j[k]$. Now we find the pdf of $|\Delta X_E[k]|$. Lemma 1 leads to

$$\lim_{k\to\infty} f(X_i[k]=x)=\frac{1}{B}\quad(0\leqslant x<B). \tag{11}$$

As UASs i and j move independently, the stationary pdf of $|\Delta X_E[k]|$ can thus be derived from Equation (11) as follows:

$$\begin{aligned}&\lim_{k\to\infty} f(|\Delta X_E[k]|=\Delta x)\\ &=2\int_0^{B-\Delta x}\lim_{k\to\infty} f(X_i[k]=x+\Delta x, X_j[k]=x)dx\\ &=2\int_0^{B-\Delta x}\lim_{k\to\infty} f(X_i[k]=x+\Delta x)f(X_j[k]=x)dx\\ &=2\int_0^{B-\Delta x}\frac{1}{B}\frac{1}{B}dx\\ &=\frac{2(B-\Delta x)}{B^2}\qquad(0\leqslant\Delta x<B).\end{aligned} \tag{12}$$

Equation (12) leads to the stationary pdf of $\Delta X[k]$, according to the relationship between cyclic distance and Euclidean distance as shown in Equation (10) and Figure 12(a):

$$\begin{aligned}&\lim_{k\to\infty} f(\Delta X[k]=\Delta x)\\ &=\lim_{k\to\infty} f(|\Delta X_E[k]|=\Delta x)+f(|\Delta X_E[k]|=B-\Delta x)\\ &=\frac{2}{B}\quad(0\leqslant\Delta x<\frac{B}{2}).\end{aligned} \tag{13}$$

The same argument leads to the uniform stationary distribution of $\Delta Y[k]$.

$$\lim_{k\to\infty} f(\Delta Y[k]=\Delta y)=\frac{2}{B}\quad(0\leqslant\Delta y<\frac{B}{2}). \tag{14}$$

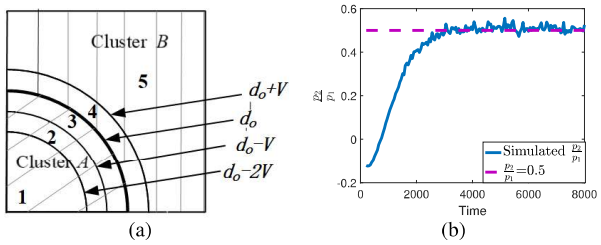

Fig. 3. (a) Partition of the state space into 5 regions based on the inter-vehicle distance. Clusters A and B are marked in different shades. (b) Illustration of the SDLAE method to find the relation between p_1 and p_2.

Since $\Delta X[k]$ and $\Delta Y[k]$ are independent, $\lim_{k\to\infty} f(D[k] = d)$ in Equation (9) can be easily derived through integration according to Figure 12(b). □

Theorem 3: Two UASs in an airspace $[0, B)^2$ *follow the RD RMM equipped with the S&S protocol. The stationary pdf of the cyclic inter-vehicle distance,* $D[k]$*, denoted as* $f_D^{S\&S}(d)$*, is bounded as follows.*

$$\begin{cases} \frac{\pi}{2} dp_{1min} < f_D^{S\&S}(d) < \frac{\pi}{2} dp_{1max}, \quad (0 \leqslant d \leqslant d_o - V) \\ \frac{\pi}{4} dp_{1max} < f_D^{S\&S}(d)) \\ < \frac{\pi}{2} dp_{1min}, \quad (d_o - V < d \leqslant d_o + V) \\ \frac{\pi}{4} dp_{1min} < f_D^{S\&S}(d) < \frac{\pi}{4} dp_{1max}, \quad (d_o + V < d \leqslant \frac{B}{2}) \\ \left(\frac{\pi}{4} - arccos\left(\frac{B}{2d}\right)\right) dp_{1\min} < f_D^{S\&S}(d) \\ < \left(\frac{\pi}{4} - arccos\left(\frac{B}{2d}\right)\right) dp_{1\max}, \quad (\frac{B}{2} < d \leqslant \frac{\sqrt{2}B}{2}) \end{cases} \tag{15}$$

where the constants $p_{1\min}$ *and* $p_{1\max}$ *are*

$$p_{1\min} = \frac{8}{\pi(d_o + V)^2 + B^2},$$
$$p_{1\max} = \frac{8}{\pi(d_o - V)^2 + B^2}.$$

Proof: We construct a Markov process with states $S^s[k] = (\Delta X[k], \Delta Y[k])$ when the two UASs move with the RD RMM equipped with the S&S protocol. The Markov chain $S^s[k]$ is aperiodic, Φ-irreducible, and Harris recurrent, and therefore, there exists a unique stationary distribution. To facilitate the analysis, we further partition the state space into five regions according to their different states transition characteristics (Figure 3(a)): Region 1 ($d \leqslant d_o - 2V$), Region 2 ($d_o - 2V < d \leqslant d_o - V$), Region 3 ($d_o - V < d \leqslant d_o$), Region 4 ($d_o < d \leqslant d_o + V$) and Region 5 ($d_o + V < d < \frac{B}{2}$). The five regions form two clusters. In Cluster A ($d \leqslant d_o$, including Regions 1, 2 and 3), one UAS moves and the other stops. In Cluster B ($d > d_o$, including Regions 4 and 5), two UASs move independently according to the independent RD RMM. We further note that states in Region 1 can only transition from Cluster A, and states in Region 5 can only transition from Cluster B. States in Regions 2, 3 and 4 can transition from both clusters.

Let us first sketch the proof idea. Denote $f_S^i(s)$ as the stationary pdf of the cyclic relative position along the x and y axes in Region i, i.e., $f_S^i(s) = \lim_{k\to\infty} f(\Delta X[k] = \Delta x, \Delta Y[k] = \Delta y)$. We analyze $f_S^i(s)$ in each region respectively. To do that, we first prove that the pdfs for the states in Regions 1 and 5 ($f_S^1(s)$ and $f_S^5(s)$) are uniform, and also identify their relation. The bounds for the pdfs $f_S^2(s)$, $f_S^3(s)$ and $f_S^4(s)$ are then all derived using $f_S^1(s)$. Finally, utilizing the axiom that the sum of pdfs for all parts is 1, the lower and upper bounds of $f_S^1(s)$ are derived. The stationary inter-vehicle distance pdf and probability in Region i, denoted as $f_D^i(d)$ and P^i, can then be found through integration.

In Region 1, one UAS stops and the other moves according to the independent RD RMM. For any position (x_0, y_0) that UAS i stops at, the relative positions between two UASs along the x and y axes are then $\Delta X[k] = \min(|X_j[k] - x_0|, B - |X_j[k] - x_0|)$ and $\Delta Y[k] = \min(|Y_j[k] - y_0|, B - |Y_j[k] - y_0|)$, respectively. Since $X_j[k]$ and $Y_j[k]$ are both uniformly distributed in the limit of large time (according to Lemma 1), $\Delta X[k]$ and $\Delta Y[k]$ can be easily proved to be also uniformly distributed in the limit, following a similar argument as in the proof of Theorem 2. Hence, $f_S^1(s)$ is uniform with value denoted as p_1. The stationary inter-vehicle distance pdf $f_D^1(d)$ and its probability in Region 1, P^1, can be represented as

$$f_D^1(d) = \frac{1}{2}\pi d p_1,$$
$$P^1 = \frac{1}{4}\pi(d_o - 2V)^2 p_1. \tag{16}$$

In Region 5, since the two UASs follow the RD RMM independently, the stationary inter-vehicle relative positions along the x and y axes are also uniformly distributed according to Theorem 2. Denote the value of $f_S^5(s)$ as p_2. The stationary inter-vehicle distance pdf $f_D^5(d)$ and its probability, P^5, can then be represented as

$$f_D^5(d) = \frac{1}{2}\pi d p_2,$$
$$P^5 = (\frac{B^2}{4} - \frac{1}{4}\pi(d_o + V)^2) p_2. \tag{17}$$

Next we find the relationship between p_1 and p_2, or $f_S^1(s)$ and $f_S^5(s)$. The most direct method is to solve the pdf $f_S(s)$ from the following equation.

$$f_S(s) = \int f(s', s) f_S(s') ds', \tag{18}$$

where $f(s', s)$ is the state transition probability kernel, representing the transition probability density from state s' to s. $f(s', s)$ in the RD RMM equipped with the S&S protocol is a piecewise function. $f(s', s)$ is a constant, i.e., $\frac{1}{2\pi}$, when $(\Delta x^2 + \Delta y^2)^{\frac{1}{2}} \leqslant d_o$, and $s' = (\Delta x', \Delta y')$ and $s = (\Delta x, \Delta y)$ satisfy $\left((\Delta x - \Delta x')^2 + (\Delta y - \Delta y')^2\right)^{\frac{1}{2}} = V$. When $(\Delta x^2 + \Delta y^2)^{\frac{1}{2}} > d_o$, $f(s', s)$ is contributed by the movements of both UASs, and can be derived using the intersection area of two circles of radius V centered at the two UASs, which is complicated to find.

We here use a numerical approach named stationary density look ahead estimator (SDLAE) [31], [32] to find the relationship between p_1 and p_2. For the discrete-time Markov process

representation of relative position $S[k]$, the marginal pdf of $S[k]$, represented by Φ_k, satisfies

$$\Phi_{k+1}(s) = \int f(s', s)\Phi_k(s')ds'. \tag{19}$$

Using the marginal density look ahead estimator (MDLAE) [31], [32], $\Phi_k(s)$ can be approximated as

$$\Phi_k^n(s) := \frac{1}{n}\sum_{j=1}^{n} f(S^j[k-1], s), \tag{20}$$

where $S^j[k-1]$, $j \in \{1, 2, \ldots, n\}$ are n independent samples drawn from the lagged state $S[k-1]$ with the pdf $\Phi_{k-1}^n(s)$. Similarly, the stationary pdf Φ_∞ is approximated as

$$\Phi_\infty^n(s) = \lim_{k\to\infty}\frac{1}{n}\sum_{j=1}^{n} f(S^j[k], s'), \tag{21}$$

where $S[k]|_{k=1}^{\infty}$ is a time series simulated from $f(s', s)$ and an arbitrary $S[1]$. Notice that $\lim_{n\to\infty}\Phi_\infty^n(s) = f_S(s)$ holds with probability 1. Using this SDLAE approach, the relation between p_1 and p_2 converges to (as shown in Figure 3(b))

$$p_1 = 2p_2. \tag{22}$$

Note that $f_S^i(s)$ is determined uniquely by the transition density kernel $f(s', s)$ as stated in Equation (18), and the relation between p_1 and p_2 is determined uniquely by the relation between the two transition kernels in Regions 1 and 5. The transition kernels in Regions 1 and 5 can be regarded as a "one-step" transition and a "two-steps" transition respectively, and is not a function of any parameters (e.g., the airspace size B, and the sensing distance d_o). As such, the relation between p_1 and p_2 is also fixed (i.e., not a function of parameters B and d_o), and would not be changed with the parameters.

Then we derive the upper and lower bounds for the stationary inter-vehicle distance distribution in Regions 2, 3, and 4 using the following steps. Step 1: we prove that $f_S^2(s)$ is uniform with density p_1 based on the Markov transition properties. Step 2: through analyzing the source states in Region 3 that transition to Region 2, we express the upper bound of $f_S^3(s)$ using p_1. Steps 3 and 4: following a similar approach, we prove that p_2 and p_1 are the lower and upper bounds of $f_S^4(s)$. In Step 5, utilizing the bounds in Region 4, we prove that p_2 is the lower bound for $f_S^3(s)$.

Step 1: Find $f_S^2(s)$. Consider all the points $s' = (\Delta x', \Delta y')$ of distance V to a point $s = (\Delta x, \Delta y)$ that satisfies $d \in [d_o - 3V, d_o - 2V)$ in Region 1, i.e., $\left((\Delta x - \Delta x')^2 + (\Delta y - \Delta y')^2\right)^{\frac{1}{2}} = V$ (marked as the circle in Figure 4(a)). As s is uniformly distributed in Region 1 with pdf p_1, at the steady-state

$$\begin{aligned} p_1 &= \int_{\widehat{aob}} f(s', s)p_1 ds' + \int_{\widehat{ab}} f(s', s) f_{S'}^2(s')ds' \\ &= f(s', s)\left(\int_{\widehat{aob}} p_1 ds' + \int_{\widehat{ab}} f_{S'}^2(s')ds'\right), \end{aligned} \tag{23}$$

where $\widehat{aob}$ represents the superior arc in Region 1 (solid curve in Figure 4(a)), and $\widehat{ab}$ represents the inferior arc in Region 2

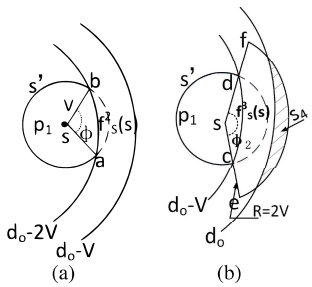

Fig. 4. (a) Illustration of Step 1. (b) Illustration of Step 2.

(dotted curve in Figure 4(a)). Equation (23) holds because for any states s' and s in Cluster A, $f(s', s)$ is a constant.

Similarly, for states s located in $[0, d_o - 3V)$ (e.g., $\sqrt{\Delta x^2 + \Delta y^2} \in [0, d_o - 3V)$) in Region 1, we have

$$p_1 = \oint f(s', s)p_1 ds' = f(s', s)\oint p_1 ds', \tag{24}$$

where $\oint$ is the integration sign over the whole circle satisfying $\left((\Delta x - \Delta x')^2 + (\Delta y - \Delta y')^2\right)^{\frac{1}{2}} = V$. As Equation (23) holds for any angle $\phi \in [0, \phi_{max})$ (shown in Figure 4(a)), where $\phi_{max} = 2arccos\frac{-V}{2(d_o-2V)}$, and any state $s = (\Delta x, \Delta y)$ satisfying $\sqrt{\Delta x^2 + \Delta y^2} \in [d_o - 3V, d_o - 2V)$. The term-to-term comparison between Equations (23) and (24) leads to

$$f_S^2(s) = p_1. \tag{25}$$

Step 2: Find the upper bound of $f_S^3(s)$. Consider all the points that can transition to $s = (\Delta x, \Delta y)$ in Region 2. Since $f_S^2(s) = p_1$, $f_S^2(s)$ satisfies the following equation, based on the Markov transition properties (Figure 4(b)),

$$\begin{aligned} p_1 = \frac{2\pi - \phi_2}{2\pi}p_1 + \int_{\widehat{cd}} f(s', s) f_{S'}^3(s') \\ + \int_{S_4} f(s', s) f_{S'}^4(s')ds', \end{aligned} \tag{26}$$

where ϕ_2 is the central angle decided by the state and V as shown in Figure 4(b). The last part in Equation (26) represents the transition probability from Region 4 (shaded region in Figure 4(b)), which is non-negative. This is because states in Region 4 can change a maximum distance of $2V$ at each time instance to reach s. As this equation holds for any ϕ_2 and any s in Region 2, a comparison between Equations (24) and (26) leads to

$$f_S^3(s) < p_1. \tag{27}$$

Steps $3-5$ prove that $f_S^3(s)$ is lower bounded by p_2 and $f_S^4(s)$ is lower bounded by p_2 and upper bounded by p_2. The proofs are documented in the Appendix.

To summarize, $f_S^i(s)$ in all regions satisfy

$$\begin{cases} f_S^i(s) = p_1 & 0 \leqslant d < d_o - V, \\ p_2 < f_S^i(s) < p_1 & d_o - V \leqslant d < d_o + V, \\ f_S^i(s) = p_2 & d_o + V \leqslant d < \frac{B}{2}. \end{cases} \tag{28}$$

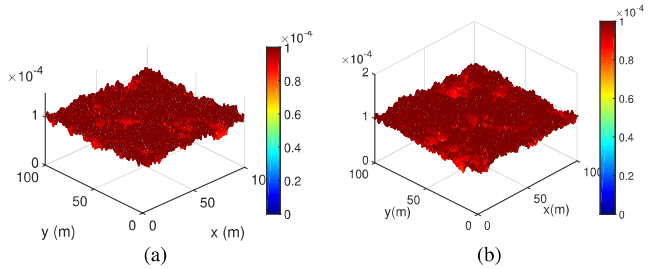

Fig. 5. Location distribution of (a) the independent RD RMM, and (b) the RD RMM equipped with the S&S protocol.

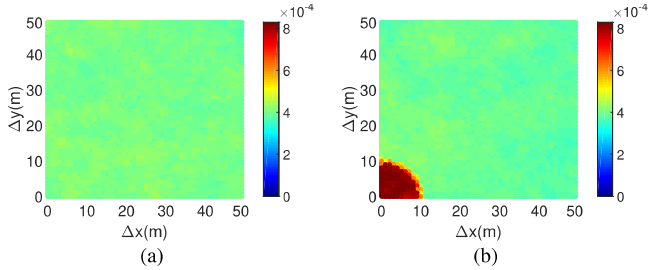

Fig. 6. Inter-vehicle relative position distribution of (a) the independent RD RMM, and (b) the RD RMM equipped with the S&S protocol.

The stationary probability P^i in each region can thus be derived through integration. Utilizing $p_1 = 2p_2$ and the axiom that $\sum_i P^i = 1$, the bounds for p_1 can be found as

$$\frac{8}{\pi(d_o+V)^2+B^2} < p_1 < \frac{8}{\pi(d_o-V)^2+B^2}. \quad (29)$$

The stationary inter-vehicle distance distribution $f_D^{S\&S}(d)$ can be derived by integrating $f_S^i(s)$ in Equations (28) and (29). Simple algebra leads to Equation (15). □

Remark 2: Theorem 2 and Theorem 3 indicate that the S&S protocol impacts the UAS inter-vehicle distance distribution. When the S&S protocol is in place, the inter-vehicle distance distribution is no more uniform.

Theorem 3 finds the bounds on the stationary distance distribution for UASs of the RD RMM equipped with S&S protocol, i.e., $f_D^{S\&S}(d)$. We show in the next section that these bounds on $f_D^{S\&S}(d)$ are indispensable in deriving the stationary collision probabilities of UASs, from which the effectiveness of different S&A protocols can be analyzed and the limits of airspace capacities are derived.

C. Numerical Illustration

We conduct simulation studies to illustrate and validate the above theoretical results. Two UASs follow the independent RD RMM, i.e., Equations (2) and (3), and the RD RMM equipped with S&S protocol, i.e., Equations (5) and (6), respectively. The airspace size is $100 \times 100\ m^2$, and UAS velocity is $1m/s$. UASs are initially randomly distributed, and choose their heading directions uniformly from $[0, 2\pi)$ at every time point $1s, 2s, 3s, \cdots$. The sensing distance is set as $10m$. We record the locations, relative positions along x and y axes, and cyclic distances of the two UASs at each time instant. To approximate the location distribution, we divide the airspace into 100×100 grids, and count the number of UASs in each grid for the entire 100000 seconds. As shown in Figures 5(a) and 5(b), the stationary location distributions for both cases are uniform.

We then simulate the inter-vehicle relative position distribution along the x and y axes for both cases. The results are shown in Figure 6. The distribution of inter-vehicle relative position for the independent RD RMM is uniform, while the RD RMM equipped with the S&S protocol is not uniform any more.

Finally, we simulate the inter-vehicle distance distribution. For the independent RD RMM, $f_D^b(d)$ increases in proportion to the distance below $\frac{B}{2}$ (Figure 7(a)), as captured in Theorem 2. For the RD RMM equipped with the S&S protocol (Figure 7(b)), $f_D^{S\&S}(d)$ increases in proportion to the distance in Regions 1, 2, and 5 below $\frac{B}{2}$, but fluctuates in Regions 3 and 4 between the upper bound (red line) and lower bound (purple line), in accordance to Theorem 3. In addition, the slope in Region 5 is 0.0003854, which is half of that in Region 1, and hence further verifies $p_1 = 2p_2$.

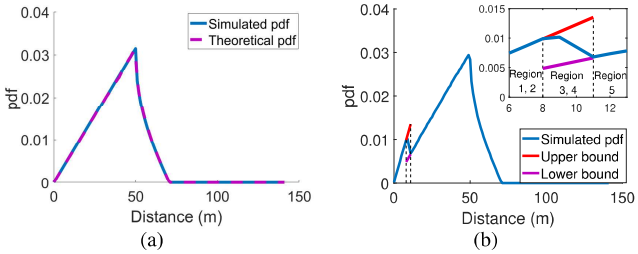

Fig. 7. Pdfs of inter-vehicle distance for (a) the independent RD RMM, (b) the RD RMM equipped with the S&S protocol.

IV. Collision Probabilities and Airspace Capacity

In this section, we first define collisions and stationary collision probabilities between a pair of UASs and then among an arbitrary number of UASs. The concept of airspace capacity follows. Based on the stationary inter-vehicle distance distributions derived in Section III-B, we analyze the stationary collision probabilities for the independent RD RMM and the RD RMM equipped with the S&S protocol. We also find the properties of airspace capacities for both RMMs.

A. Definitions

Denote the collision distance as d_c, where $0 \le d_c < d_o - V$. For a pair of UASs, the collision and stationary collision probability are defined as follows.

Definition 1: Collision occurs between a pair of UASs i and j at time k, if $D_{i,j}[k] \le d_c$. The stationary collision probability between the two UASs is defined as

$$\lim_{k\to\infty} \hat{P}_{2,i,j}[k] = \lim_{k\to\infty} P(D_{i,j}[k] \leqslant d_c). \quad (30)$$

To facilitate the comparative analysis in the rest of this sequel, we use $\lim_{k\to\infty} \hat{P}^b_{2,i,j}[k]$ and $\lim_{k\to\infty} \hat{P}^{S\&S}_{2,i,j}[k]$ to represent the stationary collision probabilities between a pair of UASs following the independent RD RMM and the RD RMM equipped with the S&S protocol, respectively.

Similarly, we define collision and stationary collision collision probability for multiple UASs.

Definition 2: Collision occurs among N UASs at time k, if and only if there exists at least one pair of UASs (denoted as i and j) satisfying $D_{i,j}[k] \leqslant d_c$. The stationary collision probability for the N UASs is thus defined as

$$\lim_{k\to\infty} \hat{P}_N[k] = \lim_{k\to\infty} P(\exists D_{i,j}[k] \leqslant d_c, i, j \in [1, N], i \neq j). \tag{31}$$

We use $\lim_{k\to\infty} \hat{P}_N^b[k]$ and $\lim_{k\to\infty} \hat{P}_N^{S\&S}[k]$ to represent the stationary collision probabilities for N UASs following the independent RD RMM and the RD RMM equipped with the S&S protocol, respectively.

We define airspace capacity based on collision probability as follows.

Definition 3: The airspace capacity N_C is defined as the maximum number of UASs with the stationary collision probability not exceeding a pre-defined threshold $\hat{P}_t$:

$$N_C = \arg\max_N \{\lim_{k\to\infty} \hat{P}_N[k] \leqslant \hat{P}_t\}. \tag{32}$$

Remark 3: The stationary collision probabilities defined in Definitions 1 and 2 provide us a good measure to compare the effectiveness of different S&A protocols. In particular, the smaller the stationary collision probability is, the more effective the S&A protocol is. Compared with transient collision probability, stationary collision probability is more suitable in evaluating S&A protocols and defining airspace capacity, as it does not rely on initial states, e.g., initial distributions of UASs. Building on the stationary collision framework, we can further study initial setups to ensure collision avoidance at all times, which we will leave to the future work.

B. Analysis

We first study the stationary collision probabilities when UASs follow the independent RD RMM, and then the RD RMM equipped with the S&S protocol. We derive the results for a pair of UASs, and then multiple UASs respectively. The analysis of airspace capacity follows.

Lemma 2: Two UASs in an airspace $[0, B)^2$ *follow the independent RD RMM. The stationary collision probability between the two UASs is*

$$\lim_{k\to\infty} \hat{P}_{2,i,j}^b[k] = \frac{\pi d_c^2}{B^2}. \tag{33}$$

Proof: According to Definition 1, the stationary collision probability between two UASs can be derived by integrating the stationary inter-vehicle distance distribution with $D_{i,j}[k] < d_c$.

$$\begin{aligned}\lim_{k\to\infty} \hat{P}_{2,i,j}^b[k] &= \int_0^{d_c} f_D^b(r)dr \\ &= \int_0^{d_c} \frac{2\pi r}{B^2}dr = \frac{\pi d_c^2}{B^2}.\end{aligned} \tag{34}$$

□

Theorem 4: Each of the N $(N > 2)$ *UASs in an airspace* $[0, B)^2$ *follows the RD RMM independently. The stationary collision probability among the* N *UASs is*

$$\lim_{k\to\infty} \hat{P}_N^b[k] = 1 - (1 - \frac{\pi d_c^2}{B^2})^{\frac{N(N-1)}{2}}, \tag{35}$$

where d_c *satisfies* $d_c \ll B$.

Proof: First we consider the case of three UASs i, j, and l moving independently according to the independent RD RMM. The collision probability among the three UASs is described according to Definition 2 as

$$\begin{aligned}&\lim_{k\to\infty} \hat{P}_3^b[k] \\ &= \lim_{k\to\infty} P(D_{i,j}[k] \leqslant d_c \cup D_{i,l}[k] \leqslant d_c \cup D_{j,l}[k] \leqslant d_c) \\ &= 1 - \lim_{k\to\infty} P(D_{i,j}[k] > d_c, D_{i,l}[k] > d_c, D_{j,l}[k] > d_c) \\ &= 1 - \lim_{k\to\infty} P(D_{j,l}[k] > d_c | D_{i,j}[k] > d_c, D_{i,l}[k] > d_c) \\ &\quad \times \lim_{k\to\infty} P(D_{i,j}[k] > d_c, D_{i,l}[k] > d_c).\end{aligned} \tag{36}$$

Note that any two of the three distances are independent, i.e., $f(D_{i,j}[k] = d_1, D_{i,l}[k] = d_2) = f(D_{i,j}[k] = d_1) f(D_{i,l}[k] = d_2)$, and the third UAS distance $D_{j,l}[k]$ can be determined by the other two distances. Therefore, Equation (36) is further written as

$$\begin{aligned}&\lim_{k\to\infty} \hat{P}_3^b[k] \\ &= 1 - \lim_{k\to\infty} P(D_{j,l}[k] > d_c | D_{i,j}[k] > d_c, D_{i,l}[k] > d_c) \\ &\quad \times \lim_{k\to\infty} P(D_{i,j}[k] > d_c) \lim_{k\to\infty} P(D_{i,l}[k] > d_c),\end{aligned} \tag{37}$$

where $\lim_{k\to\infty} P(D_{i,j}[k] > d_c)$ and $\lim_{k\to\infty} P(D_{i,l}[k] > d_c)$ can be derived from the integration of the stationary pdf ($f_D^b(d)$) shown in Equation (9), according to Theorem 2.

Then we find the conditional probability $\lim_{k\to\infty} P(D_{j,l}[k] > d_c | D_{i,j}[k] > d_c, D_{i,l}[k] > d_c)$. Because the three UASs move independently according to the RD RMM, the relative positions of the two independent UAS pairs $(\Delta X_{i,j}[k], \Delta Y_{i,j}[k])$, and $(\Delta X_{i,l}[k], \Delta Y_{i,l}[k])$ are both uniformly distributed in $[0, \frac{B}{2})^2$ according to Theorem 2.

$$\begin{aligned}\lim_{k\to\infty} f(\Delta X_{i,j}[k] = \Delta x_1, \Delta Y_{i,j} = \Delta y_1) &= \frac{4}{B^2} \\ \lim_{k\to\infty} f(\Delta X_{i,l}[k] = \Delta x_2, \Delta Y_{i,l} = \Delta y_2) &= \frac{4}{B^2},\end{aligned} \tag{38}$$

where Δx_1, Δy_1, Δx_2, and $\Delta y_2 \in [0, \frac{B}{2})$. With the relative positions, the conditional probability $\lim_{k\to\infty} P(D_{j,l}[k] > d_c | D_{i,j}[k] > d_c, D_{i,l}[k] > d_c)$ can be rewritten as

$$\begin{aligned}&\lim_{k\to\infty} P(D_{j,l}[k] > d_c | D_{i,j}[k] > d_c, D_{i,l}[k] > d_c) \\ &= \lim_{k\to\infty} P(\sqrt{\Delta X_{j,l}[k]^2 + \Delta Y_{j,l}[k]^2} > d_c | \\ &\quad \times \sqrt{\Delta X_{i,j}[k]^2 + \Delta Y_{i,j}[k]^2} > d_c, \\ &\quad \sqrt{\Delta X_{i,l}[k]^2 + \Delta Y_{i,l}[k]^2} > d_c),\end{aligned} \tag{39}$$

where $\Delta X_{j,l}[k]$ is determined by $\Delta X_{i,j}[k]$ and $\Delta X_{i,l}[k]$, and $\Delta Y_{j,l}[k]$ is determined by $\Delta Y_{i,j}[k]$ and $\Delta Y_{i,l}[k]$ considering the following four cases.

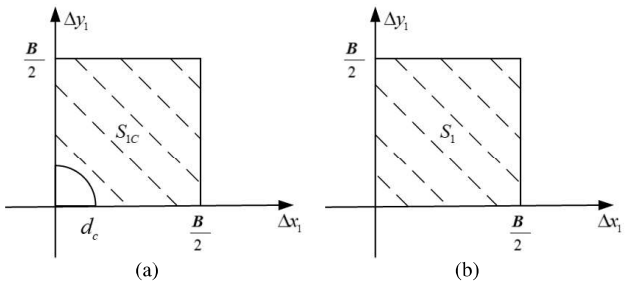

Fig. 8. The integral regions (shaded regions) of (a) S_{1C}, and (b) S_1.

Case 1, UASs j and l are on the same side of i along both x and y axes. In this case, the relative positions of j, l are $(\Delta X_{j,l}[k], \Delta Y_{j,l}[k])_1 = (|\Delta X_{i,j}[k] - \Delta X_{i,l}[k]|, |\Delta Y_{i,j}[k] - \Delta Y_{i,l}[k]|)$. Therefore, Equation (39) becomes

$$\begin{aligned}
&\lim_{k\to\infty} P(D_{j,l}[k] > d_c | D_{i,j}[k] > d_c, D_{i,l}[k] > d_c) \\
&= \lim_{k\to\infty} P\Big(\big((\Delta X_{i,j}[k] - \Delta X_{i,l}[k])^2 \\
&\quad + (\Delta Y_{i,j}[k] - \Delta Y_{i,l}[k])^2\big)^{\frac{1}{2}} > d_c | \sqrt{\Delta X_{i,j}[k]^2 + \Delta Y_{i,j}[k]^2} \\
&\quad > d_c, \sqrt{\Delta X_{i,l}[k]^2 + \Delta Y_{i,l}[k]^2} > d_c\Big) \\
&= \iint_{S_{1C}} \iint_{S_{2C}} \int_{d_c}^{\frac{B}{2}} f(\sqrt{(\Delta x_1 - \Delta x_2)^2 + (\Delta y_1 - \Delta y_2)^2} = r) \\
&\quad \times f(\Delta X_{i,j}[k] = \Delta x_1, \Delta Y_{i,j} = \Delta y_1) \\
&\quad \times f(\Delta X_{i,l}[k] = \Delta x_2, \Delta Y_{i,l} = \Delta y_2) dr ds_2 ds_1 \\
&< \iint_{S_1} \iint_{S_2} \int_{d_c}^{\frac{B}{2}} f(\sqrt{(\Delta x_1 - \Delta x_2)^2 + (\Delta y_1 - \Delta y_2)^2} = r) \\
&\quad \times f(\Delta X_{i,j}[k] = \Delta x_1, \Delta Y_{i,j} = \Delta y_1) \\
&\quad \times f(\Delta X_{i,l}[k] = \Delta x_2, \Delta Y_{i,l} = \Delta y_2) dr ds_2 ds_1 \\
&= \lim_{k\to\infty} P(D_{j,l}[k] > d_c),
\end{aligned} \tag{40}$$

where $s_1 = (\Delta x_1, \Delta y_1)$, $s_2 = (\Delta x_2, \Delta y_2)$. S_{1C} is the integral region constructed by four lines and one curve: $\Delta x_1 = 0$, $\Delta x_1 = \frac{B}{2}$, $\Delta y_1 = 0$, $\Delta y_1 = \frac{B}{2}$, and $\sqrt{\Delta x_1^2 + \Delta y_1^2} > d_c$ (marked as the shaded area in Figure 8(a)). The condition $D_{i,j}[k] > d_c$ is satisfied in S_{1C}. Similarly, S_{2C} is the region constructed by $\Delta x_2 = 0$, $\Delta x_2 = \frac{B}{2}$, $\Delta y_2 = 0$, $\Delta y_2 = \frac{B}{2}$, and $\sqrt{\Delta x_2^2 + \Delta y_2^2} > d_c$, and the condition $D_{i,l}[k] > d_c$ is satisfied in S_{2C}. S_1 is the integral region constructed by four lines: $\Delta x_1 = 0$, $\Delta x_1 = \frac{B}{2}$, $\Delta y_1 = 0$, and $\Delta y_1 = \frac{B}{2}$, and is shown as the shaded region in Figure 8(b). S_2 is the region constructed by $\Delta x_2 = 0$, $\Delta x_2 = \frac{B}{2}$, $\Delta y_2 = 0$, and $\Delta y_2 = \frac{B}{2}$.

Note that with the condition $d_c \ll B$, the conditional probability $\lim_{k\to\infty} P(D_{j,l}[k] > d_c | D_{i,j}[k] > d_c, D_{i,l}[k] > d_c)$ can be approximated by $\lim_{k\to\infty} P(D_{j,l}[k] > d_c)$ from Equation (40).

Similar analysis is applied to Case 2, where UASs j and l are on the same side of i along x axis, but on different sides of i along y axis $\big((\Delta X_{j,l}[k], \Delta Y_{j,l}[k])_2 = (|\Delta X_{i,j}[k] - \Delta X_{i,l}[k]|, |\Delta Y_{i,j}[k] + \Delta Y_{i,l}[k]|)\big)$; Case 3, where UASs j and l are on different sides side of i along x axis, but on the same side of i along y axis $\big((\Delta X_{j,l}[k], \Delta Y_{j,l}[k])_3 = (|\Delta X_{i,j}[k] + \Delta X_{i,l}[k]|, |\Delta Y_{i,j}[k] - \Delta Y_{i,l}[k]|)\big)$; and Case 4, where UASs j and l are on different sides of i along both x and y axes $\big((\Delta X_{j,l}[k], \Delta Y_{j,l}[k])_4 = (|\Delta X_{i,j}[k] + \Delta X_{i,l}[k]|, |\Delta Y_{i,j}[k] + \Delta Y_{i,l}[k]|)\big)$.

Combining Equations (37) and (40), under the condition $d_c \ll B$, the collision probability among three UASs moving according to the independent RD RMM is

$$\begin{aligned}
\lim_{k\to\infty} \hat{P}_3^b[k] &= 1 - \lim_{k\to\infty} P(\forall D_{i,j}[k] > d_c, i, j \in [1,3], i \neq j) \\
&= 1 - (1 - \lim_{k\to\infty} \hat{P}_{2,i,j}^b[k])^3.
\end{aligned} \tag{41}$$

For the N UASs case, there are a total of $\frac{N(N-1)}{2}$ inter-vehicle distance pairs, and $N-1$ of them are independent. Following a similar argument, it can be proven that under the condition $d_c \ll B$, the stationary collision probability among N UASs with the independent RD RMM is

$$\begin{aligned}
\lim_{k\to\infty} \hat{P}_N^b[k] &= \lim_{k\to\infty} P(\exists D_{i,j}[k] \leqslant d_c, i, j \in [1,N], i \neq j) \\
&= 1 - \lim_{k\to\infty} P(\forall D_{i,j}[k] > d_c, i, j \in [1,N], i \neq j) \\
&= 1 - (1 - \lim_{k\to\infty} \hat{P}_{2,i,j}^b[k])^{\frac{N(N-1)}{2}}.
\end{aligned} \tag{42}$$

Substituting Equation (33) into Equation (42), the stationary collision probability among N UASs is obtained. □

The next lemma studies the stationary collision probabilities for a couple of UASs that follow the RD RMM equipped with the S&S protocol.

Lemma 3: Two UASs in an airspace $[0, B)^2$ follow the RD RMM equipped with the S&S protocol. The stationary collision probability between the two UASs is upper bonded by

$$\lim_{k\to\infty} \hat{P}_{2,i,j}^{S\&S}[k] < \frac{2\pi d_c^2}{\pi (d_o - V)^2 + B^2}. \tag{43}$$

Proof: Integrating the upper bound of stationary inter-vehicle distance distribution in Theorem 3, we obtain

$$\begin{aligned}
\lim_{k\to\infty} \hat{P}_{2,i,j}^{S\&S}[k] &= \int_0^{d_c} \frac{\pi r}{2} p_1 dr \\
&< \frac{2\pi d_c^2}{\pi (d_o - V)^2 + B^2}.
\end{aligned} \tag{44}$$

□

In the case of multiple UASs, the independence assumption among UAS pairs is removed when the S&A protocol is in place. Therefore, the collision probability among multiple UASs is not equal to a simple multiplication of the collision probabilities between each UAS pair. In the next theorem, we derive its upper bound.

Theorem 5: N UASs in a airspace $[0, B)^2$ follow the RD RMM equipped with the S&S protocol. The stationary collision probability among the N UASs is upper bounded by

$$\lim_{k\to\infty} \hat{P}_N^{S\&S}[k] < \frac{N(N-1)}{2} \frac{2\pi d_c^2}{\pi (d_o - V)^2 + B^2}. \tag{45}$$

Proof: According to Definition 2, collision occurs among N UASs when there exists at lease one pair of UASs satisfying

$$D_{i,j}[k] \leqslant d_c.$$

$$\begin{aligned}
&\lim_{k\to\infty} \hat{P}_N^{S\&S}[k] \\
&\quad = \lim_{k\to\infty} P(\exists D_{i,j}[k] \leqslant d_c, i, j \in [1, N], i \neq j) \\
&\quad = \lim_{k\to\infty} P(D_{1,2}[k] \leqslant d_c \cup D_{1,3}[k] \\
&\quad \leqslant d_c \cup \ldots \cup D_{N-1,N}[k] \leqslant d_c) \\
&\quad < \lim_{k\to\infty} P(D_{1,2}[k] \leqslant d_c) + P(D_{1,3}[k] \leqslant d_c) + \ldots \\
&\qquad + P(D_{N-1,N}[k] \leqslant d_c) \\
&\quad = \binom{N}{2} \lim_{k\to\infty} \hat{P}_{N,i,j}^{S\&S}, \qquad (46)
\end{aligned}$$

where $\hat{P}_{N,i,j}^{S\&S}$ is the collision probability between UASs i and j when N ($N \geqslant 3$) UASs move in the airspace. $\binom{N}{2}$ is a 2-combination of UASs from a N UAS airspace, $\binom{N}{2} = \frac{N(N-1)}{2}$.

Here we state that $\hat{P}_{N,i,j}^{S\&S}$ can be approximated by $\hat{P}_{2,i,j}^{S\&S}$. $\hat{P}_{N,i,j}^{S\&S}$ is affected by the other UASs in the airspace. However, using the argument similar to the five region analysis in Theorem 3, we note that the existence of other UASs makes the UAS i or j be more likely to "stop" in all five regions, which extends the time duration for UASs i and j to be in these distance regions. When the increased time duration is approximately the same in all possible distances, the collision probability $\hat{P}_{N,i,j}^{S\&S}$ can well be approximated by $\hat{P}_{2,i,j}^{S\&S}$. This assumption holds as the triggering of the extra "stopping" only depends on the inter-vehicle distance between UAS i (or j) with other UASs, regardless of the inter-vehicle distance between i and j. With this approximation, combining Equations (46) and (43), the upper bound of the stationary collision probability among N UASs is derived as shown in Equation (45). □

The airspace capacities for the independent RD RMM and the RD RMM equipped with the S&S protocol are derived according to Definition 3, based on the collision probabilities.

Corollary 1: Given a threshold collision probability $\hat{P}_t$, the airspace capacity for the independent RD RMM (N_C^b) and the RD RMM equipped with the S&S protocol ($N_C^{S\&S}$) are expressed as follows.

$$N_C^b = \left\lfloor \sqrt{\frac{\log(1-\hat{P}_t)^2}{\log(1-\frac{\pi d_c^2}{B^2})} + \frac{1}{4}} + \frac{1}{2} \right\rfloor, \qquad (47)$$

$$N_C^{S\&S} > \left\lfloor \sqrt{\frac{\hat{P}_t(\pi(d_o - V)^2 + B^2)}{\pi d_c^2}} + \frac{1}{4} + \frac{1}{2} \right\rfloor, \qquad (48)$$

where $\lfloor\rfloor$ is the floor operation.

Proof: According to Definition 3, the airspace capacity can be derived from the collision probability analysis (described in Theorems 4 and 5) naturally. □

Remark 4: The analytical framework presented in this paper provides valuable insights on the effectiveness of local S&A protocols for global airspace capacity. We first study the S&S protocol because 1) it is a simple S&A protocol at the limit of a commonly-used collision avoidance maneuver – speed change [33], and 2) it mimics "Stop Sign" in ground traffic, which performs well in achieving collision avoidance for ground vehicles. We are thus motivated to study the performance of S&S for UASs with highly flexible operations. A comparison between Lemmas 2 and 3 shows that, surprisingly, the S&S protocol not only does not help to reduce congestion, but also worsens congestion for a highly variable on-demand UAS traffic. In particular, S&S can lead to increased collision probability and hence reduced airspace capacity. Intuitively, this is because the "stopping" protocol enlarges the collision duration if the other vehicle moves toward it. This result obtained through formal stochastic network analysis contributes to the literature in both dependent random mobility analysis and effective sense and avoid protocol analysis. In general, S&A protocols for ground vehicles or traditional flights may lose its effectiveness for dense UASs of highly flexible operations.

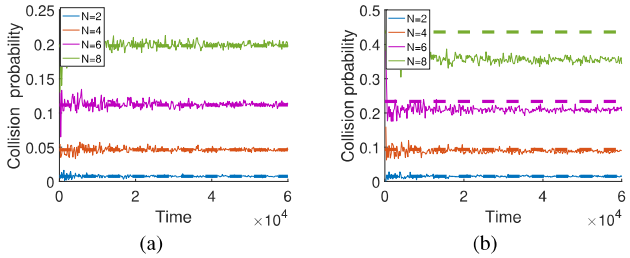

Fig. 9. Collision probabilities among UASs that follow (a) the independent RD RMM, and (b) the RD RMM equipped with the S&S protocol. The solid curves are simulated collision probabilities. The dotted lines in (a) are theoretical values, and in (b) are theoretical upper bounds.

C. Numerical Illustration

We simulate N UASs ($N = 2, 4, 6, 8$) moving in a confined square airspace ($20 \times 20\ m^2$) following the independent RD RMM with the speed of $1m/s$, and then the RD RMM equipped with the S&S. The sensing distance is set as $d_o = 2m$ and collision distance is $d_c = 1m$. Figure 9(a) suggests that the collision probability for the independent RD RMM converges in the limit of large time to the theoretical values. For the RD RMM equipped with the S&S protocol, the theoretical upper bounds characterize the collision properties (9(b)). The stationary collision probability increases with the increase of the number of UASs for both RMMs.

V. Impact Analysis of S&S Configurations

The above analytical framework allows us to systematically study the impact of local S&A protocols to global airspace capacity. In this section, we study the effect of local S&S configurations, including travel time, sensing distance, collision distance. We also compare the impacts of some other S&A protocols with the S&S protocol.

A. Impact Analysis of Travel Time

Travel time, defined as the time duration for a vehicle to hold its current heading direction [16], is one indicator of RMM randomness. UASs of different missions may have different travel time statistics. We have proved that in a 1-D airspace, travel time affects the collision probability significantly [34]. Characterizing the relationship between travel

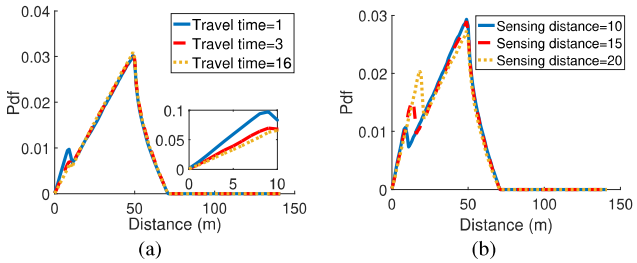

Fig. 10. Inter-vehicle distance distribution with different (a) travel time and (b) sensing distances.

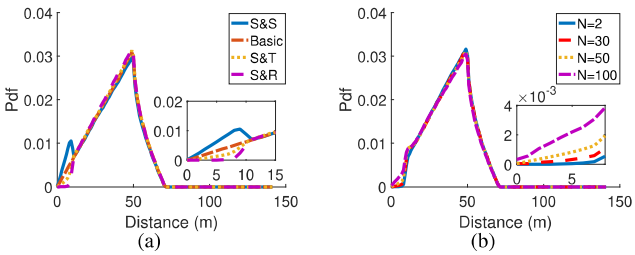

Fig. 11. Inter-vehicle distance distribution when UASs (a) follow different S&A protocols, and (b) S&R with different number of N.

time and collision probability helps us understand the effect of S&S protocols for UASs of different randomness levels.

First, we note that for the independent RD RMM, the change of travel time does not impact the joint uniform node distribution in Lemma 1 according to [15, Proposition 4.2], as well as the uniform inter-vehicle relative position distribution according to Theorem 2, or the collision probability according to Lemma 2 and Theorem 4. Hence, the airspace capacity remains the same as illustrated in Equation (47).

For the RD RMM equipped with the S&S protocol, the change of travel time also does not impact the uniform node distribution according to Theorem 1 and the same reasoning for the the independent RD RMM case. The impact of travel time to inter-vehicle distance distribution is shown in Figure 10(a), obtained using the SDLAE method. For numerical example in this section, the parameters are set as $B = 100\ m$, $d_o = 10m$, and $V = 1m/s$. Each UAS's node distribution is uniform as shown in Theorem 1. However, extending the travel time reduces the slope of inter-vehicle distance distribution in Region 1, and hence leads to reduced collision probability. In other words, less mobility randomness leads to larger airspace capacity. This observation verifies that random traffic is more difficult to address than deterministic traffic and is one major challenge to address for UTM with more flexible and uncertain vehicle mobility.

B. Impact Analysis of Sensing Distance and Collision Distance

Sensing distance is also an important parameter. Convective weather can shorten the sensing distance of UASs and affect airspace capacity [35]. This effect can be captured by reducing the parameter d_o in the S&A protocol. We here only analyze the impact of sensing distance to collision probability for the RD RMM equipped with the S&S protocol, as sensing distance does not affect the independent RD RMM. It can be seen from Figure 10(b) that longer sensing distance leads to reduced stationary collision probability in Region 1 and hence larger airspace capacity.

Collision distance, d_c, on the other hand, does not alter the inter-vehicle distance distributions for both RD RMMs. With reduced collision distance, airspace capacity increases as shown in Equations (47) and (48) for both RD RMMs.

C. Comparison With Other S&A Protocols

In this section, we compare the performance of the S&S protocol with the other two S&A protocols for the highly variable UAS traffic, including sense-and-turn-left (S&T) and sense-and-reverse (S&R).

The two protocols work as follows: when the inter-vehicle distance between two UASs is greater than the sensing distance, the two UASs follow the RD RMM independently. When the distance between them is smaller than the sensing distance, the vehicle to the relative right continues its original movement, and the vehicle to the relative left turns left for the S&T protocol, and reverses its direction for the S&R protocol, until the inter-vehicle distance is greater than the sensing distance again. The inter-vehicle distance distributions between a UAS pair for the independent RD and the RD with the S&S, S&T, and S&R are plotted in Figure 11(a). Clearly, both the S&T and S&R protocols reduce the collision probability and lead to larger airspace capacity compared to the independent RD model. Furthermore, the S&R has the best collision avoidance capabilities among them all.

Now we further study the properties of S&R. In order to evaluate the local S&R's impact to collision probability and airspace capacity, we further plot the key metric, $\hat{P}_{N,i,j}$ with the increase of number of UASs in the airspace, N (see Figure 11(b)). Clearly, with the increase of N, $\hat{P}_{N,i,j}$ increases, suggesting other vehicle's impact to the effectiveness of the local protocol.

VI. Conclusion and Future Works

In this paper, we proposed a modeling framework that equips RMMs with S&A protocols to quantitatively describe the highly random movement patterns of UASs subject to safety constraints. We proposed the RD RMM with the S&S protocol, and showed that the stationary node distribution remains uniform, however the inter-vehicle distance distribution is not uniform any more. Based on the Markov analysis, we provided theoretical bounds for the stationary inter-vehicle distance distribution. We further defined collisions between a pair of UASs and among multiple UASs based on inter-vehicle distance, and found the stationary collision probabilities for both the independent RD RMM and the RD RMM equipped with the S&S protocol. We further defined airspace capacity and derived it based on the stationary collision probabilities. Finally, we analyzed the impact of model configurations, including travel time, sensing distance, and collision distance based on the proposed analytical framework. In particular, airspace capacity is improved with less mobility randomness, enlarged sensing distance, and reduced collision distance. This analysis links local autonomy with global capacity, and provides insights on airspace capacity under highly flexible,

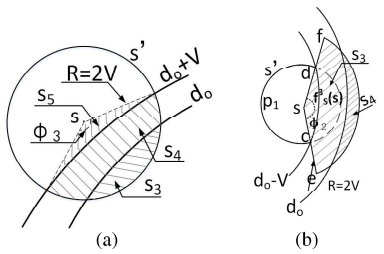

Fig. 12. (a) Illustration of Steps 3 and 4. (b) Illustration of Step 5.

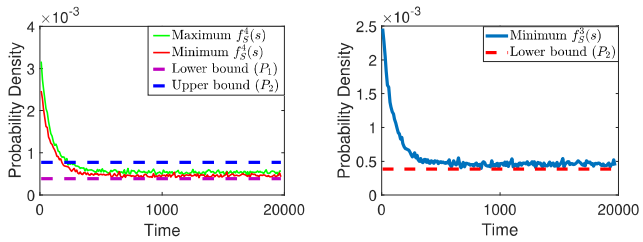

Fig. 13. SDLAE method to show the relation between (a) $f_S^4(s)$ and p_1 in Step 4, and (b) $f_S^3(s)$ and p_2 in Step 5.

variable, and uncertain mobility patterns of UASs. We found that the S&S protocol is not effective for UASs of highly variable flight patterns. Compared to the independent RD RMM, it increases collision probability and reduces airspace capacity. The S&R and S&T protocols are more effective in increasing airspace capacity. The S&R performs the best among the three, however its performance is reduced with the increase of UASs in the airspace. In the future, we will extend our study to 3-D airspace and further study the properties of RMMs and S&A protocols. We will also evaluate heterogeneous traffic and consider the impact of uncertain environment to collision and airspace capacity metrics. In addition, we will extend the stationary analysis developed in this paper to transient collision probabilities to ensure collision avoidance at all times.

APPENDIX

Proofs of Steps $3-5$ for Theorem 3.

Step 3: *Find the lower bound for* $f_S^4(s)$. Consider all the points that can transition a maximum of $2V$ to the point $s = (\Delta x, \Delta y)$ that satisfies $d \in [d_o + V, d_o + 2V)$ in Region 5 (Figure 12(a)). As s is uniformly distributed in Region 5 with pdf p_2, the following equation holds in the limit of large time.

$$p_2 = \frac{2\pi - \phi_3}{2\pi} p_2 + \int_{s_5} p_2 f(s', s) + \int_{s_4} f_S^4(s) f(s', s) ds', \tag{49}$$

where ϕ_3 is the angle determined by the states' position and the boundary of Region 4, s_4 and s_5 are the regions marked in different shades in Figure 12(a).

Similarly, for the states that are located in Region 5 and can solely transition from Region 5, we have

$$p_2 = \oint f(s', s) p_2 ds', \tag{50}$$

where the integration is for the whole area inside the circle, satisfying $\left((\Delta x - \Delta x')^2 + (\Delta y - \Delta y')^2\right)^{\frac{1}{2}} \leqslant 2V$. The comparison between Equations (49) and (50) leads to the conclusion that

$$f_S^4(s) > p_2. \tag{51}$$

Step 4: *Find the upper bound for* $f_S^4(s)$. As $p_1 = 2p_2$, Equation (50) can be further written as

$$\begin{aligned} p_2 &= \frac{2\pi - \phi_3}{2\pi} p_2 + \int_{s_3+s_4+s_5} p_2 f(s', s) ds' \\ &= \frac{2\pi - \phi_3}{2\pi} p_2 + \int_{s_5} p_2 f(s', s) ds' + \int_{s_4} \frac{1}{2} p_1 f(s', s) ds' \\ &\quad + \int_{s_3} \frac{1}{2} p_1 f(s', s) ds'. \end{aligned} \tag{52}$$

With the inequality that $\int_{s_3} p_1 f(s', s) ds' < \int_{s_4} p_1 f(s', s) ds'$, Equation (52) becomes

$$\begin{aligned} p_2 &< \frac{2\pi - \phi_3}{2\pi} p_2 + \int_{s_5} p_2 f(s', s) ds' + 2 \int_{s_4} \frac{1}{2} p_1 f(s', s) ds' \\ &= \frac{2\pi - \phi_3}{2\pi} p_2 + \int_{s_5} p_2 f(s', s) ds' + \int_{s_4} p_1 f(s', s) ds'. \end{aligned} \tag{53}$$

Comparing Equations (49) and (53), we can conclude that

$$f_S^4(s) < p_1. \tag{54}$$

Note that $f(s', s)$ is not a constant, instead, it is a function of s'. As such, it is hard to directly show $\int_{s_3} p_1 f(s', s) ds' < \int_{s_4} p_1 f(s', s) ds'$ holds for all possible s'. Here we use the SDLAE approach described in Section III-B to validate that the inequality (54) holds for all s in Region 4. The simulation result is shown in Figure 13(a).

Step 5: *Find the lower bound for* $f_S^3(s)$. Revisit Equation (26). Denote the region in the loose shades in Figure 12(b) as s_3, and the region in the dense shades as s_4. Utilizing $f_S^4(s) < p_1$ (Equation (54)) and the relation that $p_1 = 2p_2$, Equation (26) can be further written as

$$p_2 < \frac{2\pi - \phi_2}{2\pi} p_2 + \frac{1}{2} \int_{\widehat{cd}} f(s', s) f_{S'}^3 ds' + \int_{s_4} f(s', s) p_2 ds'. \tag{55}$$

With the inequality that $\int_{s_4} f(s', s) p_2 ds' < \int_{s_3} f(s', s) p_2 ds'$, Equation (55) becomes

$$\begin{aligned} p_2 &< \frac{2\pi - \phi_2}{2\pi} p_2 + \frac{1}{2} \int_{\widehat{cd}} f(s', s) f_{S'}^3 ds' + \frac{1}{2} \int_{s_3+s_4} f(s', s) p_2 ds' \\ &= \frac{2\pi - \phi_2}{2\pi} p_2 + \frac{1}{2} \int_{\widehat{cd}} f(s', s) f_{S'}^3(s') + \frac{1}{2} \frac{\phi_2}{2\pi} p_2. \end{aligned} \tag{56}$$

Comparing Equations (56) and (24), we can easily concluded that

$$f_S^3(s) > p_2. \tag{57}$$

Moreover, we use the SDLAE method to validate that Equation (57) holds for all states s in Region 3. The result is shown in Figure 13(b).

REFERENCES

[1] M. Liu, Y. Wan, and F. L. Lewis, "Analysis of the random direction mobility model with a sense-and-avoid protocol," in *Proc. IEEE Globecom Workshops (GC Wkshps)*, Singapore, Dec. 2017, pp. 1–6.

[2] X. Yuan *et al.*, "Capacity analysis of UAV communications: Cases of random trajectories," *IEEE Trans. Veh. Technol.*, vol. 67, no. 8, pp. 7564–7576, Aug. 2018.

[3] I. Maza, K. Kondak, M. Bernard, and A. Ollero, "Multi-UAV cooperation and control for load transportation and deployment," in *Proc. 2nd Int. Symp. UAVs*, Reno, NV, USA, 2009, pp. 417–449.
[4] Y. Zeng, R. Zhang, and T. J. Lim, "Wireless communications with unmanned aerial vehicles: Opportunities and challenges," *IEEE Commun. Mag.*, vol. 54, no. 5, pp. 36–42, May 2016.
[5] Y. Wan, S. Fu, J. Zander, and P. Mosterman, "Transforming on-demand communications with drones: The needs, analyses, and solutions," *Homeland Secur. Today Mag.*, vol. 4, pp. 32–35, Dec. 2015.
[6] J. Chen *et al.*, "Long-range and broadband aerial communication using directional antennas (ACDA): Design and implementation," *IEEE Trans. Veh. Technol.*, vol. 66, no. 12, pp. 10793–10805, Dec. 2017.
[7] J. Gu, T. Su, Q. Wang, X. Du, and M. Guizani, "Multiple moving targets surveillance based on a cooperative network for multi-UAV," *IEEE Commun. Mag.*, vol. 56, no. 4, pp. 82–89, Apr. 2018.
[8] *Unmanned Aerial Vehicle (UAV) Market by Application, Class, System (UAV Platforms, UAV Payloads, UAV GCS, UAV Data Links, UAV Launch and Recovery Systems), UAV Type, Mode of Operation, Range, Point of Sale, MTOW, and Region—Global Forecast to 2025*, Research and Market, Gurugram, Haryana, 2018.
[9] *Code of Federal Regulations*. Accessed: Nov. 26, 2020. [Online]. Available: https://www.law.cornell.edu/cfr/text/14/91.113
[10] Y. Wan, C. Taylor, S. Roy, C. Wanke, and Y. Zhou, "Dynamic queuing network model for flow contingency management," *IEEE Trans. Intell. Transp. Syst.*, vol. 14, no. 3, pp. 1380–1392, Sep. 2013.
[11] Y. Zhou *et al.*, "Multivariate probabilistic collocation method for effective uncertainty evaluation with application to air traffic flow management," *IEEE Trans. Syst., Man, Cybern. Syst.*, vol. 44, no. 10, pp. 1347–1363, Oct. 2014.
[12] J. Krozel, M. Peters, and K. Bilimoria, "A decentralized control strategy for distributed air/ground traffic separation," in *Proc. AIAA Guid., Navigat., Control Conf. Exhib.*, Aug. 2000, pp. 1–5.
[13] V. Bulusu and V. Polishchuk, "A threshold based airspace capacity estimation method for UAS traffic management," in *Proc. Annu. IEEE Int. Syst. Conf. (SysCon)*, Apr. 2017, pp. 1–7.
[14] J. Xie, Y. Wan, J. H. Kim, S. Fu, and K. Namuduri, "A survey and analysis of mobility models for airborne networks," *IEEE Commun. Surveys Tuts.*, vol. 16, no. 3, pp. 1221–1238, 3rd Quart., 2014.
[15] P. Nain, D. Towsley, B. Liu, and Z. Liu, "Properties of random direction models," in *Proc. IEEE 24th Annu. Joint Conf. IEEE Comput. Commun. Societies.*, Miami, FL, USA Mar. 2005, pp. 1897–1907.
[16] Y. Wan, K. Namuduri, Y. Zhou, and S. Fu, "A smooth-turn mobility model for airborne networks," *IEEE Trans. Veh. Technol.*, vol. 62, no. 7, pp. 3359–3370, Sep. 2013.
[17] J. Xie, Y. Wan, B. Wang, S. Fu, K. Lu, and J. H. Kim, "A comprehensive 3-dimensional random mobility modeling framework for airborne networks," *IEEE Access*, pp. 22849–22862, 2018.
[18] T. Camp, J. Boleng, and V. Davies, "A survey of mobility models for ad hoc network research," *Wireless Commun. Mobile Comput.*, vol. 2, no. 5, pp. 483–502, 2002.
[19] C. Cho, S.-m. Jun, E. Paik, and K. Park, "Rate control for streaming services based on mobility prediction in wireless mobile networks," in *Proc. IEEE Wireless Commun. Netw. Conf.*, vol. 4, Mar. 2005, pp. 2534–2539.
[20] Z. Cheng and W. B. Heinzelman, "Exploring long lifetime routing (LLR) in ad hoc networks," in *Proc. 7th ACM Int. Symp. Modeling, Anal. Simulation Wireless Mobile Syst.*, 2004.
[21] G. Lim, K. Shin, S. Lee, H. Yoon, and J. S. Ma, "Link stability and route lifetime in ad-hoc wireless networks," in *Proc. Int. Conf. Parallel Process. Workshops*, Vancouver, BC, Canada, 2002.
[22] C. Bettstetter, "On the connectivity of ad hoc networks," *Comput. J.*, vol. 47, no. 4, pp. 432–447, Jan. 2004.
[23] Z. J. Haas, "A new routing protocol for the reconfigurable wireless networks," in *Proc. 6th Int. Conf. Universal Pers. Commun.*, San Diego, CA, USA, 1997, pp. 562–566.
[24] C. Bettstetter, "Mobility modeling in wireless networks: Categorization, smooth movement, and border effects," *ACM SIGMOBILE Mobile Comput. Commun. Rev.*, vol. 5, no. 3, pp. 55–66, Jul. 2001.
[25] B. Cook, K. Cohen, and E. H. Kivelevitch, "A fuzzy logic approach for low altitude UAS traffic management (UTM)," in *Proc. AIAA Infotech Aerosp.*, San Diego, CA, USA, Jan. 2016, p. 1905.
[26] R. Breil, D. Delahaye, L. Lapasset, and E. Féron, "Multi-agent systems to help managing air traffic structure," *J. Aerosp. Oper.*, vol. 1, pp. 1–30, Dec. 2017.
[27] *Introduction to TCSA ii: Version 7.1*, Federal Aviation Administration, Washington, DC, USA, 2011.
[28] M. J. Kochenderfer, J. E. Holland, and J. P. Chryssanthacopoulos, "Next generation airborne collision avoidance system," *Lincoln Lab. J.*, vol. 9, no. 1, pp. 17–33, 2012.
[29] L. Sedov and V. Polishchuk, "Centralized and distributed UTM in layered airspace," in *Proc. 8th Int. Conf. Res. Air Transp.*, Barcelona, Spain, Jun. 2018.
[30] S. P. Meyn and R. L. Tweedie, *Markov Chains Stochastic Stability*. Cham, Switzerland: Springer, 2012.
[31] J. Stachurski and V. Martin, "Computing the distributions of economic models via simulation," *Econometrica*, vol. 76, no. 2, pp. 443–450, Mar. 2008.
[32] S. G. Henderson and P. W. Glynn, "Computing densities for Markov chains via simulation," *Math. Oper. Res.*, vol. 26, no. 2, pp. 375–400, May 2001.
[33] J. K. Kuchar and L. C. Yang, "A review of conflict detection and resolution modeling methods," *IEEE Trans. Intell. Transp. Syst.*, vol. 1, no. 4, pp. 179–189, Dec. 2000.
[34] M. Liu and Y. Wan, "Analysis of random mobility model with sense and avoid protocols for UAV traffic management," in *Proc. AIAA Inf. Systems-AIAA Infotech Aerosp.*, Kissimmee, FL, USA, Jan. 2018, p. 76.
[35] J. Xie *et al.*, "Distance measure to cluster spatiotemporal scenarios for strategic air traffic management," *J. Aerosp. Inf. Syst.*, vol. 12, no. 8, pp. 545–563, Aug. 2015.

Mushuang Liu received the B.S. degree in electrical engineering from the University of Electronic Science and Technology of China (UESTC), Chengdu, China, in June 2016, and the Ph.D. degree in electrical engineering from The University of Texas at Arlington (UTA), Arlington, TX, USA, in May 2020. She is currently a Post-Doctoral Research Associate and an Adjunct Professor with the Department of Electrical Engineering (EE), UTA. Her current research interests include multi-agent systems (MAS), uncertain systems, distributed control, optimal control, multi-player games, graphical games, cyber-physical systems, reinforcement learning (RL), uncertainty quantification, autonomous driving, aerial wireless communications, unmanned aircraft systems (UAS) networks, and UAS traffic management (UTM).

Yan Wan (Senior Member, IEEE) received the Ph.D. degree in electrical engineering from Washington State University in 2008 and then did post-doctoral training at the University of California, Santa Barbara. She is currently a Professor of electrical engineering with The University of Texas at Arlington. Her research interests include the modeling and control of large-scale dynamical networks, cyber-physical systems, stochastic networks, learning control, networking, uncertainty analysis, algebraic graph theory, and their applications to UAV networking, UAV traffic management, epidemic spread, complex information networks, autonomous driving, and air traffic management. Her research has led to over 180 publications and successful technology transfer outcomes. She received prestigious awards, including the NSF CAREER Award, the RTCA William E. Jackson Award, the U.S. Ignite and GENI demonstration awards, the IEEE WCNC and ICCA Best Paper Award, and the Tech Titan of the Future-University Level Award.

Frank L. Lewis (Life Fellow, IEEE) received the bachelor's degree in physics/EE and the M.S.E.E. degree from Rice University, the M.S. degree in aeronautical engineering from the University of West Florida, and the Ph.D. degree from the Georgia Institute of Technology. He is currently a UTA Distinguished Scholar Professor, a UTA Distinguished Teaching Professor, and a Moncrief-O'Donnell Chair with The University of Texas at Arlington Research Institute. He works in feedback control, intelligent systems, cooperative control systems, and nonlinear systems. He is the author of seven U.S. patents, numerous journal special issues, 420 journal articles, and 20 books. He is also a member of the National Academy of Inventors. He is also a Fellow of IFAC, AAAS, the U.K. Institute of Measurement & Control, a PE Texas, and a U.K. Chartered Engineer. He received the Fulbright Research Award, the NSF Research Initiation Grant, the ASEE Terman Award, the International Neural Network Society's Gabor Award, the U.K. Inst Measurement & Control Honeywell Field Engineering Medal, the IEEE Computational Intelligence Society Neural Networks Pioneer Award, and the AIAA Intelligent Systems Award. He also received the Outstanding Service Award from the Dallas IEEE Section, selected as an Engineer of the year by Fort Worth IEEE Section. He was listed in Fort Worth Business Press Top 200 Leaders in Manufacturing. He also received the Texas Regents Outstanding Teaching Award 2013. He is also a Founding Member of the Board of Governors of the Mediterranean Control Association.

Ella Atkins (Senior Member, IEEE) received the B.S. and M.S. degrees in aeronautics and astronautics from MIT and the M.S. and Ph.D. degrees in computer science and engineering from the University of Michigan. She is currently a Professor of aerospace engineering with the University of Michigan, where she directs the Autonomous Aerospace Systems Laboratory. She is also the Editor-in-Chief of the AIAA *Journal of Aerospace Information Systems* (JAIS). She has served on the National Academy's Aeronautics and Space Engineering Board, the Institute for Defense Analysis Defense Science Studies Group, and in AIAA technical committees. She pursues research in Aerospace system autonomy and safety. She is also involved as a Technical Fellow with Collins Aerospace.

Dapeng Oliver Wu (Fellow, IEEE) received the B.E. degree in electrical engineering from the Huazhong University of Science and Technology, Wuhan, China, in 1990, the M.E. degree in electrical engineering from the Beijing University of Posts and Telecommunications, Beijing, China, in 1997, and the Ph.D. degree in electrical and computer engineering from Carnegie Mellon University, Pittsburgh, PA, USA, in 2003.

He is currently a Professor with the Department of Electrical and Computer Engineering, University of Florida, Gainesville, FL, USA. His research interests include networking, communications, signal processing, computer vision, machine learning, smart grid, and information and network security. He received the University of Florida Term Professorship Award in 2017, the University of Florida Research Foundation Professorship Award in 2009, the AFOSR Young Investigator Program (YIP) Award in 2009, the ONR Young Investigator Program (YIP) Award in 2008, the NSF CAREER Award in 2007, the IEEE Circuits and Systems for Video Technology (CSVT) Transactions Best Paper Award for Year 2001, and the best paper awards in IEEE GLOBECOM 2011 and International Conference on Quality of Service in Heterogeneous Wired/Wireless Networks (QShine) 2006. He has served as a Technical Program Committee (TPC) Chair for IEEE INFOCOM 2012, the TPC Chair for IEEE International Conference on Communications (ICC 2008) and Signal Processing for Communications Symposium, and as a member of executive committee and/or technical program committee for over 100 conferences. He was elected as a Distinguished Lecturer by IEEE Vehicular Technology Society in 2016. He has also served as the Chair for the Award Committee, and the Chair of Mobile and wireless multimedia Interest Group (MobIG), Technical Committee on Multimedia Communications, and IEEE Communications Society. He was an Elected Member of Multimedia Signal Processing Technical Committee, IEEE Signal Processing Society, from January 2009 to December 2012. He also serves as the Editor in Chief for IEEE TRANSACTIONS ON NETWORK SCIENCE AND ENGINEERING. He was the founding Editor-in-Chief of *Journal of Advances in Multimedia* from 2006 to 2008, and an Associate Editor of IEEE TRANSACTIONS ON COMMUNICATIONS, IEEE TRANSACTIONS ON SIGNAL AND INFORMATION PROCESSING OVER NETWORKS, *IEEE Signal Processing Magazine*, IEEE TRANSACTIONS ON CIRCUITS AND SYSTEMS FOR VIDEO TECHNOLOGY, IEEE TRANSACTIONS ON WIRELESS COMMUNICATIONS, and IEEE TRANSACTIONS ON VEHICULAR TECHNOLOGY. He is also a Guest-Editor of IEEE JOURNAL ON SELECTED AREAS IN COMMUNICATIONS (JSAC), Special Issue on Cross-layer Optimized Wireless Multimedia Communications and Special Issue on Airborne Communication Networks.